Geol. Mag. **151** (*5*), *2014, pp. 765–776.* © *Cambridge University Press 2013*
doi:10.1017/S0016756813000757

Mineral ages and zircon Hf isotopic composition of the Andong ultramafic complex: implications for the evolution of Mesozoic subduction system and subcontinental lithospheric mantle beneath SE Korea

GI YOUNG JEONG*, CHANG-SIK CHEONG†‡§, KEEWOOK YI†, JEONGMIN KIM†, NAMHOON KIM†, SEOK-KI KWON‖, JIAN-ZHEN GENG¶ & HUAI-KUN LI¶

*Department of Earth and Environmental Sciences, Andong National University, Andong, Gyeongsangbukdo 760-749, Republic of Korea
†Division of Earth and Environmental Sciences, Korea Basic Science Institute, 162 Yeongudanji-ro, Ochang-eup, Cheongwon-gun, Chungcheongbukdo 363-883, Republic of Korea
‡Graduate School of Analytical Science and Technology, Chungnam National University, 99 Daehangno, Yuseong, Daejeon 305-764, Republic of Korea
‖Geological Research Division, Korea Institute of Geoscience and Mineral Resources, Daejeon 305-350, Republic of Korea
¶Tianjin Institute of Geology and Mineral Resources, Tianjin 300170, China

(*Received* 21 June 2013; *accepted* 20 August 2013; *first published online* 18 October 2013)

Abstract – The Phanerozoic subduction system of the Korean peninsula is considered to have been activated by at least Middle Permian time. The geochemically arc-like Andong ultramafic complex (AUC) occurring along the border between the Precambrian Yeongnam massif and the Cretaceous Gyeongsang back-arc basin provides a rare opportunity for direct study of the pre-Cretaceous mantle wedge lying above the subduction zone. The tightly constrained SHRIMP U–Pb age of zircons extracted from orthopyroxenite specimens (222.1 ± 1.0 Ma) is indistinguishable from the Ar/Ar age of coexisting phlogopite (220 ± 6 Ma). These ages represent the timing of suprasubduction zone magmatism likely in response to the sinking of cold and dense oceanic lithosphere and the resultant extensional strain regime in a nascent arc environment. The nearly coeval occurrence of a syenite-gabbro-monzonite suite in the SW Yeongnam massif also suggests an extensional tectonic setting along the continental margin side during Late Triassic time. The relatively enriched ε_{Hf} range of dated zircons (+6.2 to −0.6 at 222 Ma) is in contrast to previously reported primitive Sr–Nd–Hf isotopic features of Cenozoic mantle xenoliths from Korea and eastern China. This enrichment is not ascribed to contamination by the hypothetical Palaeozoic crust beneath SE Korea, but is instead attributable to metasomatism of the lithospheric mantle during the earlier subduction of the palaeo-Pacific plate. Most AUC zircons show a restricted core-to-rim spread of ε_{Hf} values, but some grains testify to the operation of open-system processes during magmatic differentiation.

Keywords: ultramafic complex, zircon, U–Pb age, Hf isotopes, lithospheric mantle.

1. Introduction

Subduction systems may have operated on the Earth since Archean time, possibly in close association with the growth of the continental crust (Martin, 1986; Drummond & Defant, 1990; Martin *et al*. 2005). The formation of calc-alkaline volcanic and plutonic rocks along Pacific-type convergent plate boundaries (Ernst, 2005) is elegantly explained by the melting of the mantle wedge (or of the downgoing slab itself) in response to the flux of fluids and melts liberated from subducting oceanic lithosphere (Tatsumi, Hamilton & Nesbitt, 1986; Peacock, Rushmer & Thompson, 1994; Pearce & Peate, 1995). Additionally, petrologic and geochemical studies have shown that many on-land remnants of oceanic lithosphere (ophiolites) also formed above subduction zones and not at mid-oceanic ridges (Miyashiro, 1973; Pearce, Lippard & Roberts, 1984; Stern & Bloomer, 1992; Shervais, 2001). It is generally accepted that these suprasubduction zone mafic–ultramafic complexes formed in a nascent or re-organized arc environment prior to the development of a magmatic arc (Casey & Dewey, 1984; Hawkins *et al.* 1984; Leitch, 1984; Stern & Bloomer, 1992; Shervais, 2001). Such a complex could therefore provide direct information about the early evolution of an arc system that may not be readily attainable by study of the subsequent, more voluminous, arc granitoids or volcanic rocks.

Circum-Pacific arc magmatism has left a huge, nearly continuous granitoid chain, for example the Sierra Nevada batholith and Peninsula Range batholith

§Author for correspondence: ccs@kbsi.re.kr

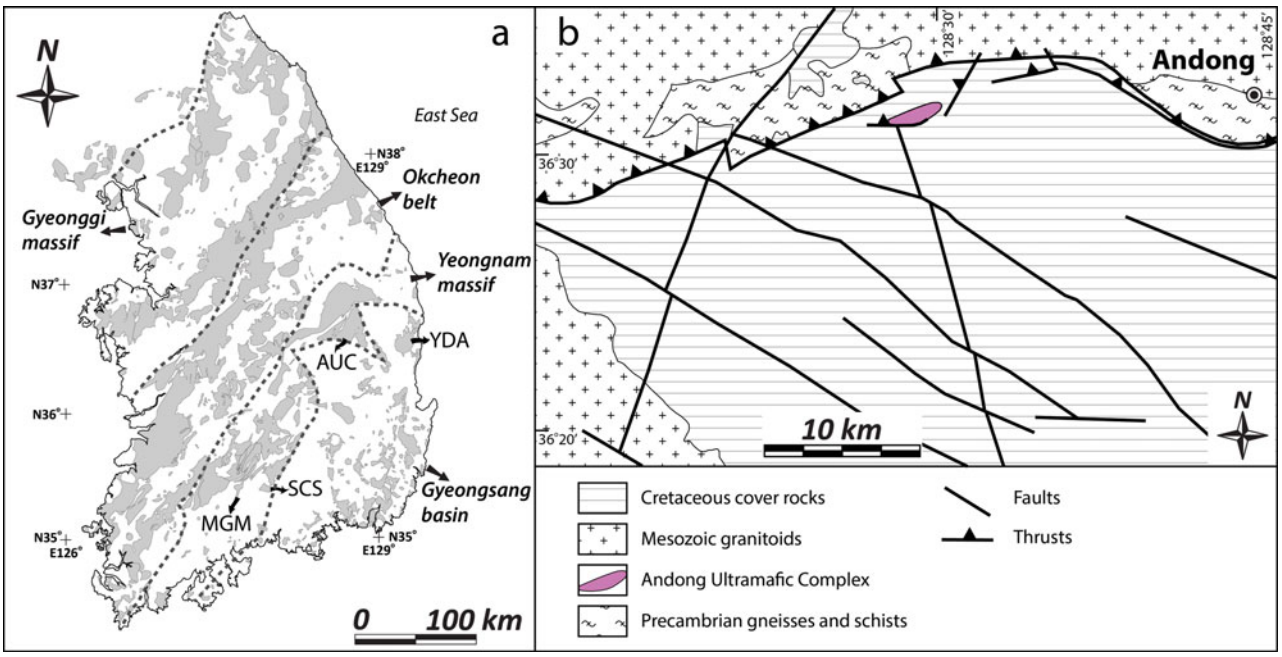

Figure 1. (Colour online) (a) Distribution of Phanerozoic granitoids in southern Korea (Cheong & Kim, 2012). AUC – Andong ultramafic complex; SCS – Sancheong syenite; MGM – Macheon gabbro-monzonite; YDA – Yeongdeok adakite. (b) Simplified geologic map of AUC and nearby areas (modified after Whattam, Cho & Smith, 2011).

in western North America, the Coastal batholith in Peru, and the East Asian granitoid belt along SE China through the Korean peninsula to Sikhote Alin in eastern Siberia. The subduction system responsible for the widespread occurrence of Phanerozoic (mostly Mesozoic) granitoids in the Korean peninsula is considered to have been activated by at least Middle Permian time (Cheong & Kim, 2012; Yi *et al*. 2012), and may be traced back to Late Carboniferous time (Kim, Ree & Kim, 2012). Although zircon Hf isotope data (Cheong *et al*. 2013) demonstrate that relatively primitive melts almost invariably participated in the genesis of these granitoids, little attention has been given to the associated mafic–ultramafic complexes, probably due to their rare occurrence.

Recently Whattam, Cho & Smith (2011) provided geochemical evidence for the magmatic formation in a suprasubduction zone setting of a peridotite and pyroxenite complex in SE Korea referred to as the Andong ultramafic complex (AUC). However, a lack of geochronological constraint hindered further discussion about how the formation of the AUC could be reasonably related to specific tectonomagmatic events that have occurred in the Korean peninsula.

We here present sensitive high-resolution ion microprobe (SHRIMP) zircon U–Pb and phlogopite Ar/Ar ages for the orthopyroxenites in the AUC, and discuss the tectonic significance of dating results in the context of Mesozoic arc evolution. We also report zircon Hf isotope data acquired by using laser-ablation multiple-collector inductively coupled plasma mass spectrometry (LA-MC-ICPMS) to delineate the source mantle characteristics. Our Hf data firstly provide a direct measure of the isotopic composition of Triassic lithospheric mantle beneath the Korean peninsula.

2. Geological background and sample description

The inland part of the southern Korean peninsula comprises two Precambrian massifs, the Gyeonggi and Yeongnam massifs, and the intervening Okcheon fold-and-thrust belt (Fig. 1). Basement rocks of the Precambrian massifs consist mainly of high-grade gneisses and schists with dominantly Late Archean – Early Proterozoic protolith ages (Lee & Cho, 2012). The southeastern marginal part of the peninsula constitutes a Cretaceous arc platform and a back-arc basin, collectively referred to as the Gyeongsang arc system (Chough & Sohn, 2010). Approximately one third of the landmass of the southern Korean peninsula consists of Permian–Palaeogene granitoids (Fig. 1), and emplacement of these granitoids is related to subduction of the palaeo-Pacific plate beneath the Eurasian plate or to continental collision between the North and South China blocks (Sagong, Kwon & Ree, 2005; Cheong & Kim, 2012). The relationship between these events and their linkage to the metamorphic and magmatic episodes are however unclear, partly because of insufficient geochronological data.

Phanerozoic arc magmatism in southern Korea appears to have begun with the intrusion of adakitic and tonalitic-trondhjemitic magmas in the northern Gyeongsang basin and central Yeongnam massif during Middle Permian – Early Triassic time (Cheong *et al*. 2011; Yi *et al*. 2012). The earlier (Late Carboniferous) subduction system was suggested by a recent detrital zircon study for the northeastern part of the Okcheon belt (Taebaeksan basin) (Kim, Ree & Kim, 2012). Southeastern Korea was subsequently subjected to extensive Early–Middle Jurassic arc magmatism (Sagong, Kwon & Ree, 2005; Kee *et al*.

https://doi.org/10.1017/S0016756813000757 Published online by Cambridge University Press

2010; Yi *et al*. 2012). The AUC lies along the border between the Yeongnam massif and the Gyeongsang basin (Fig. 1), and is structurally controlled by the east–west-trending Andong fault system that reversely transferred Precambrian–Jurassic basement rocks of the hanging wall towards the SE during Cretaceous–Palaeogene time (Choi *et al*. 2002). Lithologies of the AUC include dominant peridotites (wehrlite, plagioclase wehrlite and spinel-plagioclase wehrlite) and related serpentinites with subordinate pyroxenites (spinel-plagioclase-olivine-clinopyroxenite, spinel-plagioclase-olivine-orthopyroxenite and plagioclase-olivine websterite), gabbros (low-Ti gabbros and hornblende-biotite gabbros) and granitic dykes and sills (Whattam, Cho & Smith, 2011).

Phlogopite-bearing orthopyroxenite was discovered in the AUC by Jeong, Lee & Kwon (2012). The orthopyroxenite occurs in a *c.* 1-m-thick planar body within the serpentinite, and consists mostly of coarse subhedral to euhedral orthopyroxene crystals (>89 modal %). The chemical composition of the orthopyroxene is invariably dominated by the enstatite end-member (81.4 ± 1.2 %; Jeong, Lee & Kwon, 2012). Minor minerals include clinopyroxene (*c.* 5 %), phlogopite (*c.* 1–5 %) and plagioclase (*c.* 2 %) with trace chromian spinel, pentlandite, apatite and zircon. Clinopyroxene occurs as either exsolution lamellae or as interstitial fillings with phlogopite and plagioclase. Subhedral zircon occurs mostly interstitially or as inclusions in large orthopyroxene crystals. Reddish-brown phlogopite of 1–5 mm in size occurs in interstices of orthopyroxene crystals, which indicates late-stage crystallization. Some of the phlogopite grains were partly altered to serpentine, showing a deep green colouration. Orthopyroxene and clinopyroxene are partly altered to talc and amphibole, respectively, along grain boundaries, microcracks and cleavage planes. Plagioclase is partly altered to sericite and serpentine. We collected a relatively fresh orthopyroxenite specimen (sample SRP100) and a partly altered specimen (sample PS103). Zircons were separated from these two specimens, and fresh brown phlogopites were separated from sample SRP100.

3. Analytical details

Zircons were separated using magnetic and heavy liquid techniques and finally handpicked under a binocular microscope. Microscopic observation and SHRIMP analyses were conducted at the Korea Basic Science Institute (KBSI). Cathodoluminescence (CL) images of separated zircons were obtained using a scanning electron microscope (JEOL JSM-6610 LV). SHRIMP U–Pb dating mostly followed the analytical protocols of Williams (1998). The SL13 (U = 238 ppm) and FC1 (1099 Ma; Paces & Miller, 1993) standards were used in the analyses of uranium concentration and age calibration, respectively. Ages and concordia diagrams were produced using the Squid 2.50 and Isoplot 3.71 programs of Ludwig (2008, 2009). Weighted mean ages were calculated using ^{207}Pb-corrected $^{206}Pb^{*}/^{238}U$ ratios after excluding outliers with a statistical *t*-test, and reported at 95 % confidence.

Phlogopite grains were handpicked from the sand-size fraction of crushed orthopyroxenite. For $^{40}Ar/^{39}Ar$ dating, phlogopite grains were wrapped with pure (>99.5 %) aluminium foil and set into a sample bucket. Flux monitoring minerals (Fisher Canyon sanidine; Renne *et al*. 1998) and salt (CaF_2 and K_2SO_4) were also prepared to correct interfering isotopes during irradiation. The sample bucket was placed into an irradiation target made from pure aluminium and irradiated for three days in the IP11 position of the Hanaro reactor at the Korea Atomic Energy Research Institute. After irradiation, the samples and flux monitoring materials were placed in the glass sample chamber of the gas preparation system. The samples were heated from 600 °C to 1400 °C in vacuo with increment intervals of 25–60 °C. The extracted gas was purified and analysed with a peak-jumping method using a VG5400 mass spectrometer installed at the KBSI. Corrections for argon produced by interactions of neutrons with K and Ca were made with the following correction factors: $(^{40}Ar/^{39}Ar)_K = 3.701$, $(^{36}Ar/^{37}Ar)_{Ca} = 0.00811$ and $(^{39}Ar/^{37}Ar)_{Ca} = 0.03427$ (Tetley, McDougall & Heydegger, 1980).

Zircon Hf isotopic compositions were analysed by using a Neptune MC-ICPMS combined with an ArF excimer laser ablation system (New Wave Research) at the Tianjin Institute of Geology and Mineral Resources. The Hf isotope analyses were targeted to the dated zircon spots or new spots within the same CL domains. The laser ablation system includes a short-pulse-width (<4 ns) excimer laser operated at 193 nm with an energy density of *c.* 15 J cm^{-2}. The spot size was *c.* 50 μm. The nine Faraday collectors of the MC-ICPMS were statically aligned to simultaneously detect Yb, Lu and Hf isotopes. Details of the operational parameters are provided in Table 1. The Yb and Lu isotopic compositions employed for the correction of mass bias and isobaric interference were adopted from Vervoort *et al*. (2004) and Chu *et al*. (2002), respectively. The isobaric interference-corrected $^{176}Hf/^{177}Hf$ ratios were exponentially normalized to $^{179}Hf/^{177}Hf = 0.7325$ (Patchett *et al*. 1981). The $^{176}Lu/^{177}Hf$ and $^{176}Yb/^{177}Hf$ ratios were calculated following Iizuka & Hirata (2005). Initial epsilon Hf values were calculated by using a ^{176}Lu decay constant of 1.865×10^{-11} a^{-1} (Scherer, Münker & Mezger, 2001) and chondritic values suggested by Blichert-Toft & Albarade (1997). During the sample analysis, FC1 and GJ1 standard zircons respectively yielded average $^{176}Hf/^{177}Hf$ ratios of 0.282146 ± 0.000037 (n = 24, 1σ standard deviation, recommended value 0.282184 ± 0.000016; Woodhead & Hergt, 2005) and 0.281999 ± 0.000028 (n = 28, 1σ, recommended value 0.282003 ± 0.000018; Gerdes & Zeh, 2006). The $^{176}Lu/^{177}Hf$ and $^{176}Yb/^{177}Hf$ ratios measured for the FC-1 standard were quite scattered (0.00092 ± 0.00027 and 0.0405 ± 0.0122, 1σ), but these ratios of the GJ-1

https://doi.org/10.1017/S0016756813000757 Published online by Cambridge University Press

Table 1. LA-MC-ICPMS instrumentation and operational parameters

Parameter	Value
MC-ICPMS	
RF forward power	1139 W
RF reflected power	4 W
Cooling gas flow rate	16.0 L/min
Auxiliary gas flow rate	0.92 L/min
Sample gas flow rate	0.98 L/min
Extraction	–2000 V
Focus	–709 V
Detection system	Nine Faraday collectors
Acceleration voltage	10 kV
Interface cones	Nickel
Instrument resolution	*c.* 400
Typical sensitivity on ^{180}Hf	1–7 V (10^{11} Ω resistors)
Measurement mode	1 block of 200 cycles
Integration time	0.066 s
Laser ablation system	
Pulse rate	9 Hz
Pulse width	<4 ns
He gas flow rate	0.88 L/min
N_2 gas flow rate	0.01 L/min

standard were more tightly clustered (0.000256 ± 0.000004 and 0.00933 ± 0.00027, 1σ).

4. Results

Zircons from the two specimens (PS103 and SRP100) are very similar in shape. They are transparent, equant, stubby crystals showing subhedral development of prisms and pyramidal terminations. Grains ranging from 150 to 400 μm in length mostly show aspect ratios of less than 1:3. Many zircons occur as broken parts of whole grains. They exhibit distinct oscillatory, sector or banded zoning under CL observation and are free of inclusions or premagmatic cores. Crystal faces are rarely resorbed with the development of a thin bright CL rim. Representative CL images of the zircons are shown in Figure 2.

The SHRIMP U–Pb zircon results are listed in Table 2. The U contents range from 923 ppm to 137 ppm with a narrow range of Th/U ratios all higher than 0.57. Common lead fractions ($^{206}Pb_c$) calculated by assuming $^{206}Pb/^{238}U$–$^{207}Pb/^{235}U$ age concordance were below 2.1 %. Zircons from the two orthopyroxenites yielded indistinguishable $^{206}Pb/^{238}U$ ages of 221.7 ± 1.6 Ma (sample PS103; n = 16, mean square weighted deviation or MSWD = 1.2) and 222.5 ± 1.4 Ma (sample SRP100; n = 18, MSWD = 0.83) (Fig. 3). Because the oscillatory and sector zonings observed in CL and the relatively high Th/U ratios of the zircon provide a good indication of its magmatic origin, these ages represent the timing of zircon crystallization in a melt. The best estimate for the age of magmatism is 222.1 ± 1.0 Ma (n = 34, MSWD = 1.00), obtained by pooling all data from the two samples.

The $^{40}Ar/^{39}Ar$ age spectrum (Table 3, Fig. 4) of phlogopite from sample SRP100 shows a rough U- or saddle-shaped release pattern. The anomalously old apparent date of the fourth step (429.5 Ma) is likely due to neutron-induced recoil loss of ^{39}Ar from grain surfaces (Foland & Xu, 1990) or to the presence of contaminating phases. The spectrum does not meet the criteria for defining a plateau age, for example three or more contiguous steps constituting more than 60 % of the ^{39}Ar (Ludwig, 2008). However, steps 8–11 yield a total gas age of 220 ± 6 Ma (2σ), which is identical to the zircon SHRIMP age within error ranges. This coincidence indicates that phlogopite and zircon crystallized in the same hydrous magma. The closure temperature of the phlogopite Ar system is commonly accepted to be *c.* 450°C (Reiners & Brandon, 2006), apparently indicating rapid cooling of the magma. However, it is notable that phlogopite can retain radiogenic Ar at much

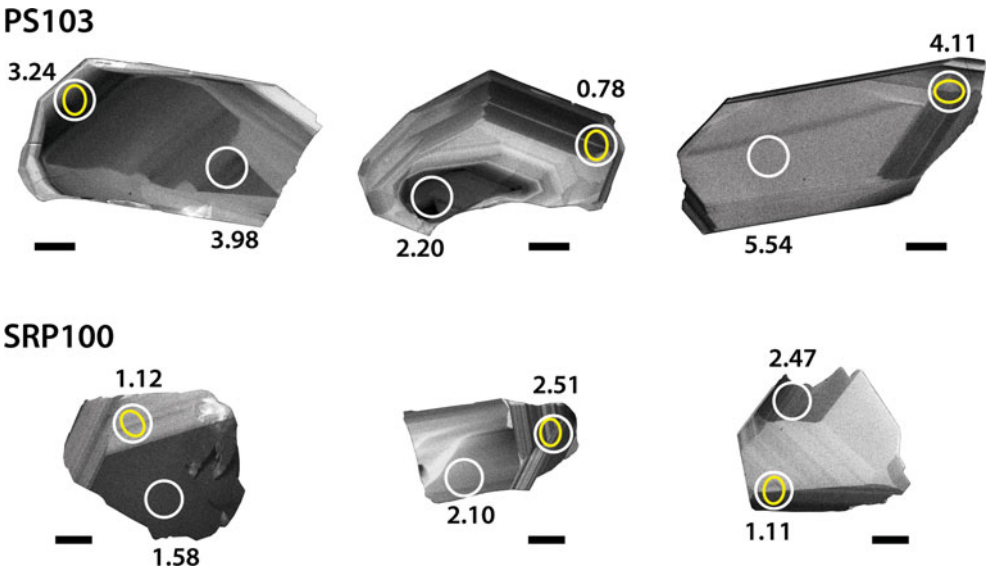

Figure 2. (Colour online) Cathodoluminescence images of selected zircon grains. Small ellipses and large circles represent the locations of points for SHRIMP dating and LA-MC-ICPMS analysis, respectively. $\varepsilon_{Hf}(t)$ values are given with the locations. All scale bars are 50 μm in length.

https://doi.org/10.1017/S0016756813000757 Published online by Cambridge University Press

Table 2. Results of SHRIMP zircon U–Th–Pb isotope analyses (Pb^*: radiogenic lead; Pb_c: common lead)

Spot	$^{206}Pb_c$ (%)	U (ppm)	Th (ppm)	$^{232}Th/^{238}U$	$^{206}Pb^*/^{238}U^\dagger$	± %	$^{207}Pb^*/^{206}Pb^*$	± %	Date (Ma)‡
1.1	0.51	259	143	0.57	0.03440	1.2	0.0483	3.1	219 ± 2
2.1	0.17	531	498	0.97	0.03507	1.2	0.0480	4.6	223 ± 2
3.1	0.57	163	137	0.87	0.03555	1.5	0.0498	6.4	225 ± 3
4.1	1.20	137	104	0.78	0.03572	1.6	0.0562	7.8	225 ± 3
5.1	0.53	271	174	0.66	0.03403	1.3	0.0463	3.8	217 ± 2
6.1	0.58	206	121	0.61	0.03563	1.4	0.0519	3.5	225 ± 3
7.1	0.49	248	181	0.75	0.03465	1.4	0.0494	4.3	220 ± 3
8.1	0.03	220	135	0.63	0.03535	1.4	0.0464	3.8	225 ± 3
9.1	0.21	923	670	0.75	0.03476	1.1	0.0486	2.5	221 ± 2
10.1	0.81	146	84	0.59	0.03454	1.5	0.0483	4.5	219 ± 3
13.1	1.14	263	162	0.64	0.03437	1.6	0.0457	6.7	219 ± 3
14.1	1.02	233	150	0.67	0.03560	1.5	0.0455	7.4	227 ± 3
15.1	0.78	321	182	0.58	0.03469	1.4	0.0486	6.1	220 ± 3
16.1	1.00	350	212	0.63	0.03496	1.4	0.0524	5.3	221 ± 3
17.1	0.83	338	289	0.88	0.03441	2.5	0.0452	11.9	220 ± 4
18.1	1.90	162	102	0.65	0.03535	1.7	0.0509	11.0	224 ± 3
1.1	1.87	155	114	0.76	0.03510	1.9	0.0553	10.2	221 ± 3
2.1	1.16	272	205	0.78	0.03487	1.5	0.0551	4.3	220 ± 3
3.1	0.68	609	574	0.97	0.03435	1.3	0.0473	5.3	219 ± 2
4.1	0.94	343	211	0.64	0.03481	1.4	0.0477	3.6	221 ± 3
6.1	0.78	206	154	0.77	0.03472	1.6	0.0472	5.9	221 ± 3
7.1	1.78	147	141	0.99	0.03577	2.0	0.0569	15.3	225 ± 3
8.1	1.17	142	109	0.79	0.03610	1.7	0.0578	6.3	227 ± 3
9.1	1.22	244	141	0.60	0.03455	1.4	0.0507	3.8	219 ± 3
10.1	0.87	217	135	0.64	0.03486	2.0	0.0428	9.8	223 ± 3
11.1	0.67	275	196	0.73	0.03492	1.4	0.0496	4.3	222 ± 3
12.1	1.47	161	105	0.67	0.03571	1.6	0.0538	8.2	225 ± 3
14.1	1.37	165	129	0.81	0.03539	1.6	0.0488	6.5	225 ± 3
15.1	2.12	145	98	0.69	0.03551	3.5	0.0564	10.3	223 ± 7
16.1	1.94	142	95	0.69	0.03569	1.6	0.0631	6.9	223 ± 3
17.1	0.19	840	496	0.61	0.03546	1.1	0.0518	2.8	224 ± 2
18.1	1.02	230	156	0.70	0.03499	1.5	0.0495	6.0	222 ± 3
19.1	1.91	137	100	0.76	0.03588	1.6	0.0641	7.0	223 ± 3
20.1	1.22	181	129	0.74	0.03602	1.8	0.0506	8.6	228 ± 3

† common lead corrected by ^{207}Pb
‡ ^{207}Pb corrected $^{206}Pb^*/^{238}U$ age

higher temperature when nearly all of the K and Ar are partitioned into this phyllosilicate structure (Kelley & Wartho, 2000), as is presumably the case for our analysed orthopyroxenite sample.

Table 4 lists the LA-MC-ICPMS Hf–Yb–Lu isotopic data of zircon. The $^{176}Hf/^{177}Hf$ and $^{176}Lu/^{177}Hf$ ratios and the Late Triassic age constrained here yielded initial ε_{Hf} values (222.1 Ma) ranging from +6.2 to −0.6. Zircons from sample SRP100 had slightly lower initial ε_{Hf} values (1.7 ± 1.1; 1σ) than those from sample PS103 (3.4 ± 1.2; 1σ). The $^{176}Lu/^{177}Hf$ (0.00014–0.00090) and $^{176}Yb/^{177}Hf$ (0.0055–0.0371) ratios of the zircons are positively correlated with each other ($R^2 = 0.97$).

5. Discussion

5.a. Change in Triassic subduction mode

The prominent enrichment of fluid-mobile elements (Cs, Rb, Ba, Th, U, K, light rare earth elements, Pb and Sr) and depletion of high-field-strength elements (Nb, Zr and Ti) in the AUC ultramafic rocks (Whattam, Cho & Smith, 2011; Jeong, Lee & Kwon, 2012) are indicative of subduction-related fluid enhancement in the mantle source (Pearce, 1982; Ellam & Hawkesworth, 1988; Brenan *et al*. 1995; Ayers, Dittmer & Layne, 1997), which led Whattam, Cho & Smith, (2011) to suggest that the AUC formed in a supra-subduction zone. This interpretation is reminiscent of the hinge rollback model (Stern & Bloomer, 1992) in which new oceanic crust forms in response to the sinking of old, cold and dense oceanic lithosphere, which leaves a gap fed by melts flowing upwards from the asthenosphere shortly after the initiation of subduction. The rock assemblage of the AUC (wehrlites, pyroxenites and primitive gabbros) is typically associated with ongoing melting of a refractory mantle wedge (Shervais, 2001). Subduction of old, thick lithosphere results in a relatively steep subduction zone, an extensional regime in the overlying plate (Jarrard, 1986), trench retreat and oceanwards migration of arc magmatism. A Late Triassic extensional tectonic setting in SE Korea is implicitly supported by the intrusion of the Sancheong syenite (Rb–Sr whole-rock age = 211 ± 23 Ma, initial $^{87}Sr/^{86}Sr$ = 0.70598 ± 0.00060; Park *et al*. 2006) and the Macheon gabbro-monzonite (thermal ionization mass spectrometry U–Pb zircon age = 223 ± 3 Ma; Kim & Turek, 1996; SHRIMP zircon age = 236.8 ± 3.4 Ma, Kim *et al.* 2011*b*) in the southwestern part of the Yeongnam massif (Fig. 1). The nascent arc environment responsible for the formation of the AUC does not appear to have reached maturity during the Triassic because subsequent intrusion of the calc-alkaline intrusive suite did not occur in SE Korea until Early Jurassic time (Park, Lee & Cheong, 2005; Kee *et al*. 2010; Yi *et al*. 2012). Alternatively,

https://doi.org/10.1017/S0016756813000757 Published online by Cambridge University Press

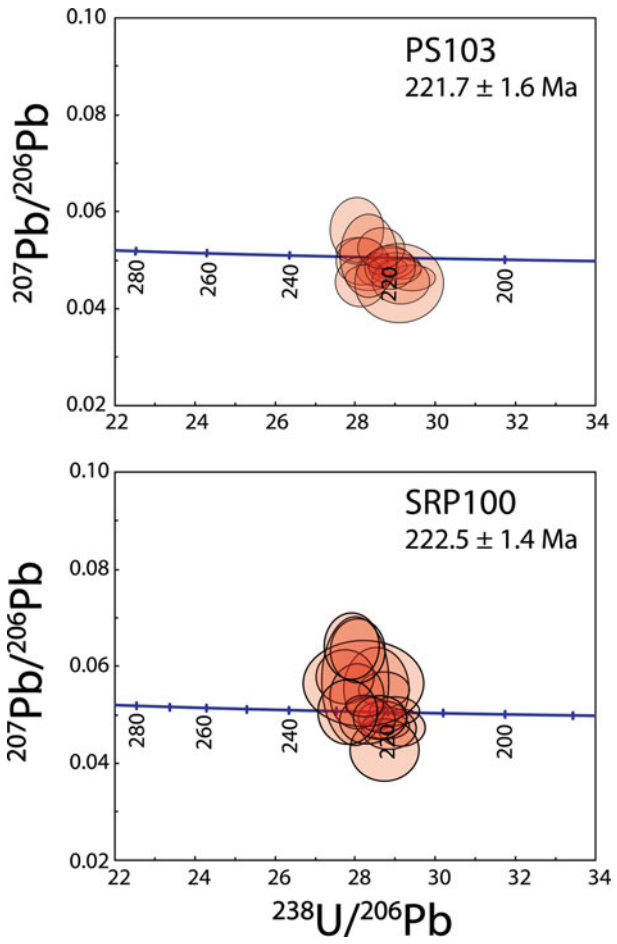

Figure 3. (Colour online) Zircon concordia diagrams with mean ^{207}Pb-corrected ^{206}Pb/^{238}U ages. Error ellipses are at the 1σ level. Data points represent ^{208}Pb-corrected ratios.

the change in the angle of convergence, convergence rate, subduction angle or their combination may have resulted in this magmatic gap.

The Late Triassic 'Mariana'-type (Uyeda & Kanamori, 1979) subduction mode suggested in this study is in striking contrast to the hot subduction mode envisioned from the occurrence of adakite to the east of the AUC (Fig. 1) in the Permian–Triassic transition period (Cheong, Kwon & Sagong, 2002; Yi *et al*. 2012). Geochemical characteristics of the Yeongdeok adakite such as distinctly high La/Yb (37.5–114.6) and Sr/Y (138.2–214.0) (Cheong, Kwon & Sagong, 2002) are consistent with the signatures of high-silica adakites (Martin *et al*. 2005). Adakites are apparently restricted to hot subduction regimes having anomalously high heat flow that allows the subducted slab to melt rather than dehydrate. Subduction of young and hot lithosphere is the most widely accepted environment for the formation of adakites (Defant & Drummond, 1990; Martin, 1999). Yi *et al*. (2012) suggested that subduction of the palaeo-Pacific ridge may have provided the additional heat to the arc system necessary to produce the Yeongdeok adakite. The development of a new subduction system in Late Triassic time, suggested by this study, may have been preceded by arc–arc or arc–continent collision. The geological records of these tectonic events may still remain in SE Korea or else have been erased by the intense Jurassic–Cretaceous magmatic overprints subjected to this region. In fact, arc–continent collision yielded very diverse tectonic architectures due to the complexities of involved continental margin and arc–trench complex, as revealed by studies on modern arcs (Brown *et al.* 2011). Further studies are needed to test our suggestion of the Permian–Triassic change in the subduction mode. Calc-alkaline granitoids were emplaced in the central Yeongnam massif after intrusion of the Yeongdeok adakite but before the onset of a new high-angle subduction (Kim *et al*. 2011*b*). This seemingly continuous Early–Middle Triassic arc magmatism is in contrast to a magmatic gap from 260 to 190 Ma in the SE coastal region of China, which is possibly attributed to flat slab subduction (Li & Li, 2007; Li *et al*. 2012).

Our interpretation is not compatible with a recent tectonic model suggested by the detrital zircon ages of modern river sediments (Choi, Lee & Orihashi, 2012), in which continuous subduction angle increase and resultant slab rollback were the driving forces of apparent Triassic south-eastward arc migration in southern Korea (249–202 Ma). Note, however, that Triassic granitic magmatism in central and SE Korea occurred under different tectonic environments, that is, post-collisional stabilization of tectonically overthickened crust in the former region (Cho, Lee & Armstrong, 2008; Williams, Cho & Kim, 2009; Kim *et al*. 2011*a*, *b*) and subduction of the palaeo-Pacific plate in the

Table 3. ^{40}Ar/^{39}Ar data of phlogopite from sample SRP100

ID	Temp (°C)	^{40}Ar/^{39}Ar	^{37}Ar/^{39}Ar	^{36}Ar/^{39}Ar	K/Ca	^{40}Ar* (%)	^{39}Ar (%)	Age (Ma)
R100–2	650	348.3	0.72	0.86	1.35	26	1.0	16.0
R100–4	800	2456.1	0.68	5.80	1.44	30	0.8	126.7
R100–5	860	2835.0	1.82	0.70	0.52	93	0.8	429.5
R100–6	920	1322.5	0.18	0.03	5.64	99	9.5	214.6
R100–7	960	1250.5	0.15	0.01	6.74	100	10.4	204.7
R100–8	990	1364.8	0.08	0.01	12.22	100	14.6	221.9
R100–9	1010	1326.9	0.09	0.01	10.57	100	13.5	216.1
R100–10	1035	1357.9	0.09	0.01	10.82	100	14.5	220.9
R100–11	1060	1366.2	0.13	0.01	7.89	100	11.0	222.4
R100–12	1110	1196.6	0.10	0.01	9.81	100	13.5	196.0
R100–13	1150	1365.9	–0.03	0.01	–33.31	100	6.1	221.2
R100–14	1210	1637.8	0.21	0.01	4.73	100	4.1	264.3

https://doi.org/10.1017/S0016756813000757 Published online by Cambridge University Press

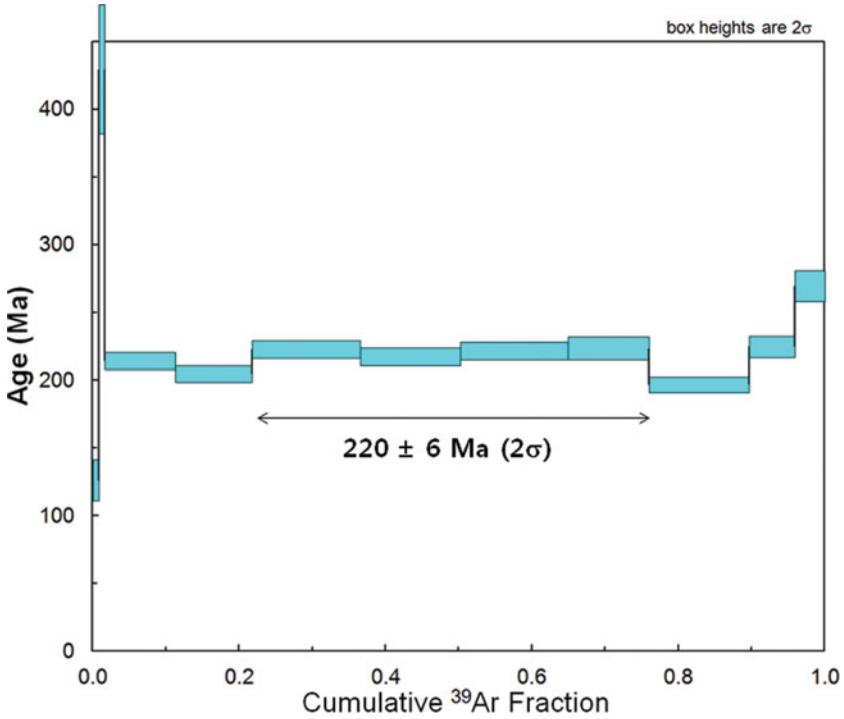

Figure 4. (Colour online) $^{40}Ar/^{39}Ar$ age spectrum of phlogopite from sample SRP100.

latter region (Cheong, Kwon & Sagong, 2002; Cheong *et al*. 2011; Yi *et al*. 2012). By detrital zircon ages alone, it is not possible to ascertain the tectonic environment of the host granitoids in which the zircons originally crystallized.

5.b. Zircon Hf isotopic constraints

According to Whattam, Cho & Smith (2011), the AUC wehrlites and pyroxenites formed by fractional crystallization and accumulation processes, respectively, in suprasubduction zone magmas derived from a refractory mantle residue that underwent a high degree of melt extraction.

Geochemical and mineralogical studies have examined mantle xenoliths hosted by Cenozoic alkali basalts that ubiquitously occur in the Korean peninsula (Choi, 2012), but information about the pre-Cenozoic mantle lithosphere is quite restricted because of the lack of Mesozoic or Palaeozoic mantle xenoliths on the peninsula. These Cenozoic xenoliths are unexceptional spinel peridotites without hydrous minerals or garnet, which is indicative of a relatively thin (25–90 km; Park, 2010) subcontinental lithospheric mantle (SCLM) beneath the peninsula. Choi *et al*. (2005) and Choi & Mukasa (2012) reported their primitive Sr–Nd–Hf isotopic compositions (whole-rock $^{87}Sr/^{86}Sr = 0.704542$–$0.702346$, clinopyroxene $^{143}Nd/^{144}Nd = 0.513858$–$0.512712$, clinopyroxene $^{176}Hf/^{177}Hf = 0.285092$–$0.283196$) similar to Sr–Nd compositions of the fertile peridotite xenoliths derived from post-Archean lithospheric mantle in eastern China. The clinopyroxene $\varepsilon_{Hf}(t)$ values of the peridotite xenoliths hosted by Cenozoic alkali basalts in the eastern North China craton (Shandong Province) have also been reported to be consistently depleted mantle-like or more juvenile (mostly $>+15$; Chu *et al*. 2009). Our Hf isotope data for AUC zircons indicate that the Late Triassic lithospheric mantle beneath SE Korea was distinctly more enriched than the primitive Cenozoic mantle beneath Korea and eastern China.

Zircon ε_{Hf} values of the AUC orthopyroxenites were plotted on a crystallization time versus ε_{Hf} diagram (Fig. 5), together with previous data for the Permian–Palaeogene granitoids occurring within the Gyeongsang basin (Cheong *et al*. 2013). From zircon Hf data of the granitoids, Cheong *et al*. (2013) postulated a hypothetical Early Palaeozoic crust beneath SE Korea whose recycling yielded Cretaceous–Palaeogene granitoids. As shown in Figure 5, the AUC zircon data plot well below the depleted-mantle trend and the evolution line regressed by the granitoid data, ruling out the possibility that the lower ε_{Hf} values resulted from contamination by the Palaeozoic crustal protolith. Instead, the Late Triassic Hf isotopic enrichment of the lithospheric mantle is most likely attributable to melt or fluid addition during the course of prior subduction of the palaeo-Pacific plate that has occurred in SE Korea since Late Palaeozoic time (Cheong *et al*. 2011; Kim *et al*. 2011*b*; Yi *et al*. 2012). The primitive Sr–Nd–Hf isotopic compositions of Cenozoic mantle xenoliths from Korea and eastern China indicate that the SCLM beneath SE Korea returned to a juvenile signature after Late Triassic time. This recovery is also evidenced by whole-rock and mineral geochemical data indicating secondary metasomatism of the AUC wehrlites by mid-ocean ridge basalt (MORB) -like asthenospheric mantle melts (Whattam, Cho & Smith, 2011).

The $\varepsilon_{Hf}(t)$ values of points on zircons were plotted against the $^{176}Lu/^{177}Hf$ ratios (Fig. 6). The core-to-rim

https://doi.org/10.1017/S0016756813000757 Published online by Cambridge University Press

Table 4. Results of zircon LA-MC-ICPMS Lu–Yb–Hf isotopic analyses ('core' and 'rim' refer to the relative position of the analysis point within the crystal)

Spot no.	$^{176}Hf/^{177}Hf$	2s SE	$^{176}Lu/^{177}Hf$	2s SE	$^{176}Yb/^{177}Hf$	2s SE	$\varepsilon_{Hf}(t)$
PS103 01.1 rim	0.282754	0.000016	0.0003147	0.0000005	0.010667	0.000038	4.20
PS103 01.2 core	0.282741	0.000020	0.0008130	0.0000010	0.031138	0.000023	3.66
PS103 02.1 rim	0.282728	0.000016	0.0004987	0.0000150	0.020284	0.000643	3.24
PS103 02.2 core	0.282748	0.000018	0.0003504	0.0000010	0.014839	0.000063	3.98
PS103 03.1 rim	0.282658	0.000016	0.0005081	0.0000015	0.019682	0.000032	0.78
PS103 03.2 core	0.282697	0.000015	0.0002751	0.0000027	0.010438	0.000081	2.20
PS103 04.1 rim	0.282702	0.000019	0.0005345	0.0000031	0.019786	0.000084	2.33
PS103 04.2 core	0.282755	0.000017	0.0002862	0.0000022	0.011804	0.000073	4.23
PS103 05.1 rim	0.282717	0.000020	0.0008286	0.0000025	0.029547	0.000116	2.82
PS103 05.2 core	0.282747	0.000018	0.0008160	0.0000012	0.030194	0.000071	3.89
PS103 06.1 rim	0.282770	0.000018	0.0002241	0.0000005	0.008785	0.000019	4.76
PS103 07.1 rim	0.282722	0.000018	0.0004488	0.0000018	0.017838	0.000062	3.02
PS103 07.2 core	0.282698	0.000017	0.0005884	0.0000049	0.022844	0.000181	2.18
PS103 08.1 rim	0.282715	0.000018	0.0002864	0.0000016	0.010283	0.000051	2.81
PS103 09.1 rim	0.282695	0.000018	0.0008861	0.0000007	0.030630	0.000026	2.03
PS103 10.1 rim	0.282721	0.000015	0.0002016	0.0000010	0.007682	0.000048	3.04
PS103 13.1 rim	0.282732	0.000017	0.0002242	0.0000003	0.008605	0.000010	3.41
PS103 14.1 rim	0.282758	0.000018	0.0003404	0.0000005	0.011244	0.000019	4.32
PS103 15.1 rim	0.282771	0.000022	0.0002922	0.0000010	0.010696	0.000079	4.80
PS103 15.2 core	0.282748	0.000020	0.0005958	0.0000044	0.025615	0.000170	3.94
PS103 16.1 rim	0.282673	0.000018	0.0003702	0.0000004	0.013008	0.000036	1.30
PS103 17.1 rim	0.282812	0.000018	0.0003474	0.0000009	0.014777	0.000019	6.23
PS103 17.2 core	0.282741	0.000019	0.0002060	0.0000007	0.008469	0.000030	3.75
PS103 18.1 rim	0.282751	0.000020	0.0002105	0.0000005	0.009003	0.000023	4.11
PS103 18.2 core	0.282792	0.000022	0.0002127	0.0000005	0.009259	0.000018	5.54
PS103 19.1 core	0.282735	0.000016	0.0003924	0.0000003	0.016383	0.000030	3.50
PS103 19.2 rim	0.282690	0.000015	0.0002266	0.0000002	0.009010	0.000018	1.94
PS103 20.1 core	0.282712	0.000017	0.0006314	0.0000009	0.022167	0.000024	2.66
PS103 20.2 rim	0.282733	0.000015	0.0003261	0.0000003	0.010999	0.000009	3.46
PS103 21.1 core	0.282787	0.000018	0.0004671	0.0000035	0.017585	0.000155	5.34
PS103 21.2 rim	0.282683	0.000019	0.0003236	0.0000012	0.012005	0.000037	1.67
PS103 22.1 core	0.282735	0.000020	0.0001799	0.0000003	0.007517	0.000016	3.55
PS103 22.2 rim	0.282733	0.000019	0.0004414	0.0000024	0.016539	0.000108	3.43
SRP100 01.1 rim	0.282714	0.000019	0.0001658	0.0000004	0.006732	0.000021	2.79
SRP100 02.1 rim	0.282668	0.000021	0.0005004	0.0000003	0.018032	0.000036	1.12
SRP100 02.2 core	0.282683	0.000022	0.0008964	0.0000010	0.037053	0.000064	1.58
SRP100 03.1 rim	0.282669	0.000017	0.0004008	0.0000013	0.015545	0.000047	1.17
SRP100 04.1 rim	0.282757	0.000015	0.0002650	0.0000003	0.010211	0.000007	4.29
SRP100 04.2 core	0.282666	0.000017	0.0002806	0.0000004	0.011401	0.000014	1.10
SRP100 06.1 rim	0.282642	0.000016	0.0002982	0.0000007	0.010633	0.000029	0.25
SRP100 07.1 rim	0.282678	0.000020	0.0002727	0.0000010	0.009369	0.000039	1.51
SRP100 08.1 rim	0.282645	0.000016	0.0001475	0.0000003	0.005463	0.000009	0.35
SRP100 09.1 rim	0.282707	0.000019	0.0005971	0.0000012	0.022109	0.000083	2.51
SRP100 09.2 core	0.282695	0.000017	0.0004309	0.0000011	0.016720	0.000024	2.10
SRP100 10.1 rim	0.282724	0.000016	0.0001707	0.0000015	0.006630	0.000065	3.14
SRP100 10.2 core	0.282693	0.000019	0.0003314	0.0000012	0.013729	0.000072	2.04
SRP100 11.1 rim	0.282630	0.000018	0.0002800	0.0000013	0.011249	0.000039	-0.20
SRP100 11.2 core	0.282730	0.000021	0.0008672	0.0000025	0.036677	0.000068	3.27
SRP100 12.1 rim	0.282731	0.000038	0.0004325	0.0000026	0.014480	0.000087	3.36
SRP100 14.1 rim	0.282725	0.000017	0.0002290	0.0000003	0.009144	0.000025	3.18
SRP100 14.2 core	0.282658	0.000023	0.0003535	0.0000004	0.015059	0.000032	0.79
SRP100 15.1 rim	0.282683	0.000020	0.0001371	0.0000004	0.005727	0.000021	1.72
SRP100 16.1 rim	0.282681	0.000025	0.0002998	0.0000004	0.012015	0.000017	1.62
SRP100 16.2 core	0.282673	0.000020	0.0002937	0.0000006	0.012769	0.000030	1.34
SRP100 17.1 core	0.282725	0.000019	0.0004829	0.0000019	0.019518	0.000049	3.13
SRP100 18.1 rim	0.282667	0.000021	0.0002726	0.0000008	0.011139	0.000063	1.11
SRP100 18.2 core	0.282706	0.000020	0.0004052	0.0000008	0.017387	0.000066	2.47
SRP100 19.1 rim	0.282675	0.000022	0.0002342	0.0000005	0.009024	0.000032	1.40
SRP100 19.2 core	0.282685	0.000023	0.0003455	0.0000005	0.015243	0.000026	1.76
SRP100 20.1 rim	0.282617	0.000022	0.0001901	0.0000004	0.008110	0.000010	–0.64
SRP100 21.1 rim	0.282628	0.000017	0.0001661	0.0000008	0.006586	0.000044	–0.25
SRP100 21.2 rim	0.282661	0.000016	0.0001776	0.0000008	0.006961	0.000050	0.92
SRP100 22.1 core	0.282666	0.000020	0.0002191	0.0000010	0.008838	0.000059	1.08
SRP100 22.2 rim	0.282698	0.000018	0.0001657	0.0000003	0.006395	0.000011	2.22
SRP100 23.1 core	0.282660	0.000015	0.0004136	0.0000006	0.015412	0.000009	0.86
SRP100 23.2 rim	0.282641	0.000017	0.0002897	0.0000033	0.010643	0.000127	0.21
SRP100 24.1 core	0.282676	0.000018	0.0004839	0.0000009	0.019593	0.000055	1.42
SRP100 24.2 rim	0.282697	0.000018	0.0003863	0.0000022	0.014662	0.000107	2.18
SRP100 25.1 core	0.282711	0.000017	0.0003277	0.0000003	0.013564	0.000022	2.66
SRP100 25.2 rim	0.282717	0.000021	0.0002036	0.0000004	0.008344	0.000025	2.91

https://doi.org/10.1017/S0016756813000757 Published online by Cambridge University Press

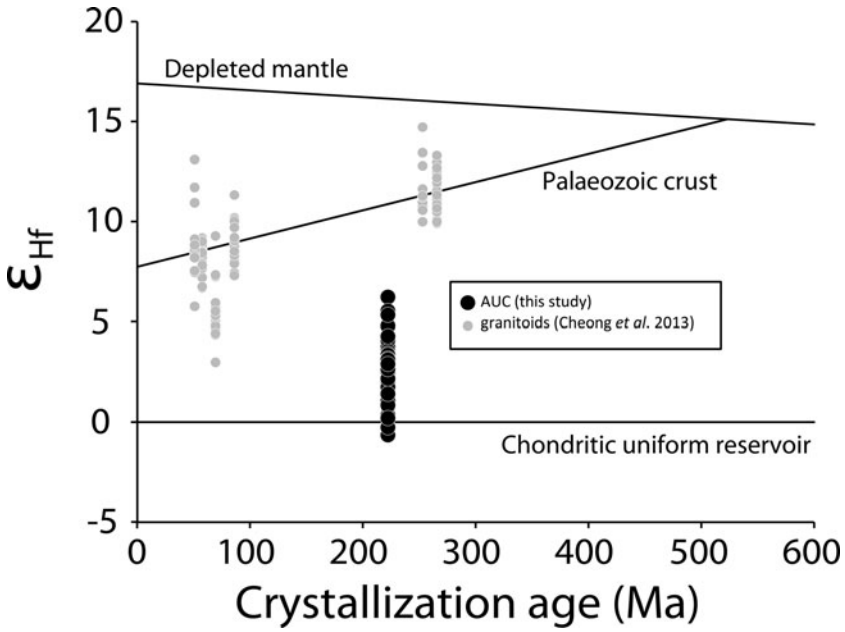

Figure 5. Plot of ε_{Hf} versus crystallization ages of zircons from the Phanerozoic granitoids within the Gyeongsang basin (Cheong *et al*. 2013) and the ACU orthopyroxenite. The evolutionary path of the depleted mantle is based on $^{176}Hf/^{177}Hf$ and $^{176}Lu/^{177}Hf$ ratios from Griffin *et al*. (2000). A regression line constructed from zircon data of the granitoids is shown for reference.

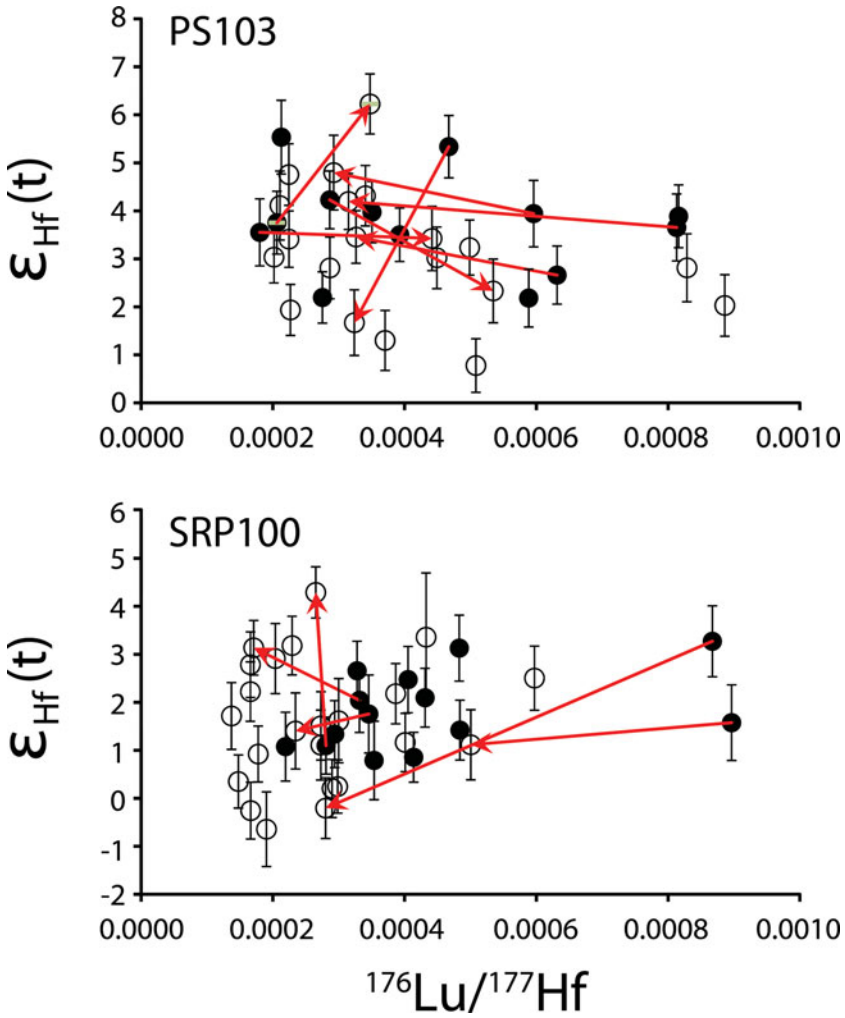

Figure 6. (Colour online) Plots of zircon $\varepsilon_{Hf}(t)$ versus the $^{176}Lu/^{177}Hf$ ratio. Core-to-rim variation is shown by arrowed tie lines connecting data from the same grain. Error bars indicate 2σ standard error. The closed and open symbols represent zircon cores and rims, respectively.

https://doi.org/10.1017/S0016756813000757 Published online by Cambridge University Press

decrease in $^{176}Lu/^{177}Hf$ ratio of SRP100 zircons could be ascribed to progressive chemical change in the melts; this trend is not prominent in zircons from sample PS103 however. Most of these zircon grains show a restricted core-to-rim spread of $\varepsilon_{Hf}(t)$ values within ±2 epsilon units, but both decreasing and increasing core-to-rim trends outside analytical uncertainty were detected for some grains. This indicates an open-system evolution of the magma system involving interaction with pre-existing crustal materials and replenishment by fresh melt inputs. The most probable candidate for the crustal contaminant is Precambrian basement rocks in the Yeongnam massif. However, the crustal contamination must have been minor in the AUC magmas considering the significantly high Ni (596–5570 ppm; Whattam, Cho & Smith, 2011) and Cr contents (1118–3872 ppm; Whattam, Cho & Smith, 2011; Jeong, Lee & Kwon, 2012) reported for the wehrlite and pyroxenite whole-rock samples and the lack of basement xenoliths in the AUC. Furthermore, the data do not show a systematic trend in Figure 6, which can be expected for the case of overall contamination by the Precambrian crust.

6. Conclusions

The zircon and phlogopite ages of this study reveal that the magmatic AUC formed in Late Triassic time, likely in response to the subduction of a dense oceanic slab during the initiation of an arc system. This cold subduction mode strikingly contrasts to the prior hot subduction mode envisioned from the occurrence of high-silica adakites that formed in the Permian–Triassic transition period. The ε_{Hf} values of AUC zircons are distinctly more enriched than primitive values of Cenozoic mantle xenoliths from eastern China and the Korean peninsula. These lower ε_{Hf} values are not attributable to contamination by the Palaeozoic crustal protolith beneath SE Korea because they plot below the evolution line formed by the zircon data of the granitoids within the Gyeongsang basin on the time–ε_{Hf} diagram. The Late Triassic Hf isotopic enrichment of the lithospheric mantle beneath SE Korea is instead most probably due to melt or fluid addition that resulted from prior subduction of the palaeo-Pacific plate. Most AUC zircons show a restricted core-to-rim spread of ε_{Hf} values; open-system behaviour, possibly associated with slight crustal contamination of the AUC magma system during magmatic differentiation, is however testified by the core-to-rim variations of some grains.

Acknowledgements. This research was supported by Korea Basic Science Institute (T33621) and National Research Foundation of Korea (NRF-2011–0028597) grants. Field work was partly supported by Korea Institute of Geoscience and Mineral Resources. LA-MC-ICPMS analysis of zircon Hf isotopes was supported by Chinese Geological Survey Project No. 12120113013900. We thank Professor Moonsup Cho and an anonymous reviewer for their detailed and constructive comments.

References

AYERS, J. C., DITTMER, S. K. & LAYNE, G. D. 1997. Partitioning of elements between peridotite and H_2O at 2.0–3.0 GPa and 900–1100 °C, and application to models of subduction zone processes. *Earth and Planetary Science Letters* **150**, 381–98.

BLICHERT-TOFT, J. & ALBARADE, F. 1997. The Lu-Hf isotope geochemistry of chondrites and the evolution of the mantle-crust system. *Earth and Planetary Science Letters* **148**, 243–56.

BRENAN, J. M., SHAW, H. F., RYERSON, F. J. & PHINNEY, D. L. 1995. Mineral-aqueous fluid partitioning of trace elements at 900 °C and 2.0 GPa: constraints on the trace element chemistry of mantle and deep crustal fluids. *Geochimica et Cosmochimica Acta* **59**, 3331–50.

BROWN, D., RYAN, P. D., AFONSO, J. C., BOUTELIER, D., BURG, J. P., BYRNE, T., CALVERT, A., COOK, F., DEBART, S., DEWEY, J. F., GERYA, T. V., HARRIS, R., HERRINGTON, R., KONSTANTINOVSKAYA, E., RESTON, T. & ZAGOREVSKI, A. 2011. Arc-continent collision: the making of an orogen. In *Arc-continent Collision* (eds D. Brown & P. D. Ryan), pp. 477–93. Springer, Heidelberg, Frontiers in Earth Science Series.

CASEY, J. F. & DEWEY, J. F. 1984. Initiation of subduction zones along transform and accreting plate boundaries, triple-junction evolution, and forearc spreading centres: implications for ophiolitic geology and obduction. In *Ophiolites and Oceanic Lithosphere* (eds I. G. Gass, S. J. Lippard & A. W. Shelton), pp. 269–90. Geological Society of London, Special Publication no. 13.

CHEONG, C.-S. & KIM, N. 2012. Review of radiometric ages for Phanerozoic granitoids in southern Korean Peninsula. *Journal of Petrological Society of Korea* **21**, 173–92 (in Korean with English abstract).

CHEONG, C.-S., KIM, N., KIM, J., YI, K., JEONG, Y.-J. & CHO, M. 2011. Permian to Triassic magmatism and metamorphism in Andong-Cheongsong-Yeongdeok area, southeastern Korea. *Geological Society of Korea Annual Meeting (Abstract Volume)*, **4** (in Korean).

CHEONG, C.-S., KWON, S.-T. & SAGONG, H. 2002. Geochemical and Sr-Nd-Pb isotopic investigation of Triassic granitoids and basement rocks in the northern Gyeongsang Basin, Korea: implications for the young basement in the East Asian continental margin. *The Island Arc* **11**, 25–44.

CHEONG, C.-S., YI, K., KIM, N., LEE, T.-H., LEE, S. R., GENG, J.-Z. & LI, H.-K. 2013. Tracking source materials of Phanerozoic granitoids in South Korea by zircon Hf isotopes. *Terra Nova* **25**, 228–35.

CHO, D.-L., LEE, S. R. & ARMSTRONG, R. 2008. Termination of the Permo-Triassic Songrim (Indosinian) orogeny in the Ogcheon belt, South Korea: occurrence of ca. 220 Ma post-orogenic alkali granites and their tectonic implications. *Lithos* **105**, 191–200.

CHOI, P. Y., LEE, S. R., CHOI, H.-I., HWANG, J.-H., KWON, S.-K., KO, I.-S. & AN, G.-O. 2002. Movement history of the Andong Fault System: geometric and tectonic approaches. *Geosciences Journal* **6**, 91–102.

CHOI, S. H. 2012. Lithospheric mantle beneath the Korean peninsula: implications from peridotite xenoliths in alkali basalts. *Journal of Petrological Society of Korea* **21**, 235–47 (in Korean with English abstract).

CHOI, S. H., KWON, S.-T., MUKASA, S. B. & SAGONG, H. 2005. Sr–Nd–Pb isotope and trace element systematics of mantle xenoliths from Late Cenozoic alkaline lavas, South Korea. *Chemical Geology* **221**, 40–64.

CHOI, S. H. & MUKASA, S. B. 2012. Lu–Hf and Sm–Nd isotope systematics of Korean spinel peridotites: a case

for metasomatically induced Nd–Hf decoupling. *Lithos* **154**, 263–76.

CHOI, T., LEE, Y. I. & ORIHASHI, Y. 2012. Mesozoic detrital zircon U-Pb ages of modern river sediments in Korea: implications for migration of arc magmatism in the Mesozoic East Asian continental margin. *Terra Nova* **24**, 156–65.

CHOUGH, S. K. & SOHN, Y. K. 2010. Tectonic and sedimentary evolution of a Cretaceous continental arc-backarc system in the Korean peninsula: new view. *Earth Science Reviews* **101**, 225–49.

CHU, N. C., TAYLOR, R. N., CHAVAGNAC, V., NESBITT, R. W., BOELLA, M. & MILTON, J. A. 2002. Hf isotope ratio analysis using multi-collector inductively coupled plasma mass spectrometry: an evaluation of isobaric interference corrections. *Journal of Analytical Atomic Spectrometry* **17**, 1567–74.

CHU, Z.-Y., WU, F.-Y., WALKER, R. J., RUDNICK, R. L., PITCHER, L., PUCHTEL, I. S., YANG, Y.-H. & WILDE, S. A. 2009. Temporal evolution of the lithospheric mantle beneath the eastern North China Craton. *Journal of Petrology* **50**, 1857–98.

DEFANT, M. J. & DRUMMOND, M. S. 1990. Derivation of some modern arc magmas by melting of young subducted lithosphere. *Nature* **347**, 662–5.

DRUMMOND, M. S. & DEFANT, M. J. 1990. A model for trondhjemite-tonalite-dacite genesis and crustal growth via slab melting: Archaean to modern comparisons. *Journal of Geophysical Research* **95B**, 21503–21.

ELLAM, R. M. & HAWKESWORTH, C. J. 1988. Elemental and isotopic variations in subduction related basalts: evidence for a three component model. *Contributions to Mineralogy and Petrology* **98**, 72–80.

ERNST, W. G. 2005. Alpine and Pacific styles of Phanerozoic mountain building: subduction-zone petrogenesis of continental crust. *Terra Nova* **17**, 165–88.

FOLAND, K. A. & XU, Y. 1990. Diffusion of ^{40}Ar and ^{39}Ar in irradiated orthoclase. *Geochimica et Cosmochimica Acta* **54**, 3147–58.

GERDES, A. & ZEH, A. 2006. Combined U–Pb and Hf isotope LA-(MC-)ICP-MS analyses of detrital zircons: comparison with SHRIMP and new constraints for the provenance and age of an Armorican metasediment in Central Germany. *Earth and Planetary Science Letters* **249**, 47–61.

GRIFFIN, W. L., PEARSON, N. J., BELOUSOVA, E. A., JACKSON, S. E., O'REILLY, S. Y., VAN ACHTERBERG, E. & SHEE, S. R. 2000. The Hf isotope composition of cratonic mantle: LAM-MC-ICPMS analysis of zircon megacrysts in kimberlites. *Geochimica et Cosmochimica Acta* **64**, 133–47.

HAWKINS, J. W., BLOOMER, S. H., EVANS, C. A. & MELCHIOR, J. T. 1984. Evolution of intra-oceanic arc-trench systems. *Tectonophysics* **102**, 175–205.

IIZUKA, T. & HIRATA, T. 2005. Improvements of precision and accuracy in in-situ Hf isotope microanalysis of zircon using the laser ablation-MC-ICPMS technique. *Chemical Geology* **220**, 121–37.

JARRARD, R. D. 1986. Relations among subduction parameters. *Reviews of Geophysics* **24**, 217–83.

JEONG, G. Y., LEE, S. R. & KWON, S.-K. 2012. Phlogopite-bearing orthopyroxenite in Andong ultramafic complex. *Journal of Mineralogical Society of Korea* **25**, 249–61 (in Korean with English abstract).

KEE, W.-S., KIM, S. W., JEONG, Y.-J. & KWON, S. 2010. Characteristics of Jurassic continental arc magmatism in South Korea: tectonic implications. *The Journal of Geology* **118**, 305–23.

KELLEY, S. P. & WARTHO, J.-A. 2000. Rapid kimberlite ascent and the significance of Ar-Ar ages in xenolith phlogopites. *Science* **289**, 609–11.

KIM, C.-B. & TUREK, A. 1996. Advances in U-Pb zircon geochronology of Mesozoic plutonism in the southwestern part of Ryeongnam massif, Korea. *Geochemical Journal* **30**, 323–38.

KIM, H. S., REE, J.-H. & KIM, J. 2012. Tectonometamorphic evolution of the Permo-Triassic Songrim (Indosinian) orogeny: evidence from the late Paleozoic Pyeongan Supergroup in the northeastern Taebaeksan Basin, South Korea. *International Journal of Earth Sciences* **101**, 483–98.

KIM, J., YI, K., JEONG, Y.-J. & CHEONG, C.-S. 2011*a*. Geochronological and geochemical constraints on the petrogenesis of Mesozoic high-K granitoids in the central Korean peninsula. *Gondwana Research* **20**, 608–20.

KIM, S. W., KWON, S., KOH, H. J., YI, K., JEONG, Y.-J. & SANTOSH, M. 2011*b*. Geotectonic framework of Permo-Triassic magmatism within the Korean Peninsula. *Gondwana Research* **20**, 865–89.

LEE, S. R. & CHO, K. 2012. Precambrian crustal evolution of the Korean peninsula. *Journal of Petrological Society of Korea* **21**, 89–112 (in Korean with English abstract).

LEITCH, E. C. 1984. Island arc elements and arc-related ophiolites. *Tectonophysics* **106**, 177–203.

LI, Z.-X. & LI, X.-H. 2007. Formation of the 1300-km-wide intracontinental orogen and postorogenic magmatic province in Mesozoic South China: a flat-slab subduction model. *Geology* **35**, 179–82.

LI, Z.-X., LI, X.-H., CHUNG, S.-L., LO, C.-H., XU, X. & LI, W.-X. 2012. Magmatic switch-on and switch-off along the South China continental margin since the Permian: transition from an Andean-type to a Western pacific-type plate boundary. *Tectonophysics* **532–5**, 271–90.

LUDWIG, K. R. 2008. *User's Manual for Isoplot 3.6: A Geochronological Toolkit for Microsoft Excel*. Berkeley: Berkeley Geochronology Center Special Publication.

LUDWIG, K. R. 2009. *User's Manual for SQUID 2*. Berkeley: Berkeley Geochronology Center Special Publication.

MARTIN, H. 1986. Effect of steeper Archaean geothermal gradient on geochemistry of subduction-zone magmas. *Geology* **14**, 753–6.

MARTIN, H. 1999. Adakitic magmas: modern analogues of Archaean granitoids. *Lithos* **46**, 411–29.

MARTIN, H., SMITHIES, R. H., RAPP, R., MOYEN, J.-F. & CHAMPION, D. 2005. An overview of adakite, tonalite–trondhjemite–granodiorite (TTG) and sanukitoid: relationships and some implications for crustal evolution. *Lithos* **79**, 1–24.

MIYASHIRO, A. 1973. The Troodos ophiolitic complex was probably formed in an island arc. *Earth and Planetary Science Letters* **19**, 218–24.

PACES, J. B. & MILLER JR., J. D. 1993. Precise U–Pb ages of duluth complex and related mafic intrusions, northeastern Minnesota: geochronological insights to physical, petrogenetic, paleomagnetic, and tectonomagmatic processes associated with the 1.1 Ga midcontinent rift system. *Journal of Geophysical Research: Solid Earth* **98**, 13997–4013.

PARK, K.-H. 2010. Evolution of the subcontinental lithospheric mantle of Korean peninsula: partial loss and its timing. *Journal of Petrological Society of Korea* **19**, 199–208 (in Korean with English abstract).

PARK, K.-H., KIM, D.-Y., SONG, Y.-S. & CHEONG, C.-S. 2006. Rb-Sr isotopic composition of Mesozoic Sancheong syenite and its geologic implication. *Journal of*

Petrological Society of Korea **15**, 1–9 (in Korean with English abstract).

PARK, K.-H., LEE, H.-S. & CHEONG, C.-S. 2005. Sphene U-Pb ages of the granodiorites from Gimcheon, Seongju and Anui areas of the middle Yeongnam massif. *Journal of Petrological Society of Korea* **14**, 1–11 (in Korean with English abstract).

PATCHETT, P. J., KOUVO, O., HEDGE, C. E. & TATSUMOTO, M. 1981. Evolution of continental crust and mantle heterogeneity: evidence from Hf isotopes. *Contributions to Mineralogy and Petrology* **78**, 279–97.

PEACOCK, S. M., RUSHMER, T. & THOMPSON, A. B. 1994. Partial melting of subducting oceanic crust. *Earth and Planetary Science Letters* **121**, 227–44.

PEARCE, J. A. 1982. Trace element characteristics of lavas from destructive plate boundaries. In *Andesites* (eds J. S. Thorpe), pp. 525–48. New York: John Wiley.

PEARCE, J. A., LIPPARD, S. J. & ROBERTS, S. 1984. Characteristics and tectonic significance of supra-subduction zone ophiolites. In *Marginal Basin Geology: Volcanic and Associated Sedimentary and Tectonic Processes in Modern and Ancient Marginal Basins* (eds B. P. Kokelaar & M. F. Howells), pp. 74–94. Geological Society of London, Special Publication no. 16.

PEARCE, J. A. & PEATE, D. W. 1995. Tectonic implications of the composition of volcanic arc lavas. *Annual Review of Earth and Planetary Science* **23**, 251–85.

REINERS, P. W. & BRANDON, M. T. 2006. Using thermochronology to understand orogenic erosion. *Annual Reviews of Earth and Planetary Science* **34**, 219–66.

RENNE, P. R., SWISHER, C. C., DEINO, A. L., KARNER, D., OWENS, T. L. & DEPAOLO, D. J. 1998. Intercalibration of standards, absolute ages and uncertainties in $^{40}Ar/^{39}Ar$ dating. *Chemical Geology* **145**, 117–52.

SAGONG, H., KWON, S.-T. & REE, J.-H. 2005. Mesozoic episodic magmatism in South Korea and its tectonic implication. *Tectonics* **24**, TC5002, published online 13 September 2005, doi:10.1029/2004TC001720.

SCHERER, E., MÜNKER, C. & MEZGER, K. 2001. Calibration of the lutetium-hafnium clock. *Science* **293**, 683–7.

SHERVAIS, J. W. 2001. Birth, death, and resurrection: the life cycle of suprasubduction zone ophiolites. *Geochemistry, Geophysics, Geosystems* **2**, published online 31 January 2011, doi:10.1029/2000GC000080.

STERN, R. J. & BLOOMER, S. H. 1992. Subduction zone infancy: examples from the Eocene Izu-Bonin-Mariana and Jurassic California arcs. *Geological Society of America Bulletin* **104**, 1621–36.

TATSUMI, Y., HAMILTON, D. L. & NESBITT, R. W. 1986. Chemical characteristics of fluid phase released from a subducted lithosphere and origin of arc magmas: evidence from high-pressure experiments and natural rocks. *Journal of Volcanology and Geothermal Research* **29**, 293–309.

TETLEY, N., MCDOUGALL, I. & HEYDEGGER, H. R. 1980. Thermal neutron interference in the $^{40}Ar/^{39}Ar$ dating technique. *Journal of Geophysical Research* **85**, 7201–5.

UYEDA, S. & KANAMORI, H. 1979. Back-arc opening and the mode of subduction. *Journal of Geophysical Research* **84**, 1049–61.

VERVOORT, J. D., PATCHETT, P. J., SÖDERLUND, U. & BAKER, M. 2004. Isotopic composition of Yb and the determination of Lu concentrations and Lu/Hf ratios by isotope dilution using MC-ICPMS. *Geochemistry, Geophysics, Geosystems* **5**, published online 2 November 2002, doi: 10.1029/2004GC000721.

WHATTAM, S. A., CHO, M. & SMITH, E. M. 2011. Magmatic peridotites and pyroxenites, Andong Ultramafic Complex, Korea: geochemical evidence for supra-subduction zone formation and extensive melt–rock interaction. *Lithos* **127**, 599–618.

WILLIAMS, I. S. 1998. U–Th–Pb geochronology by ion microprobe. In *Applications of Microanalytical Techniques to Understanding Mineralizing Processes* (eds M. A. McKibben, W. G. III Shanks & W. I. Ridley), pp. 1–35. Society of Economic Geologists, Littleton, Colorado, Reviews in Economic Geology 7.

WILLIAMS, I. S., CHO, D.-L. & KIM, S. W. 2009. Geochronology, and geochemical and Nd–Sr isotopic characteristics, of Triassic plutonic rocks in the Gyeonggi Massif, South Korea: constraints on Triassic post-collisional magmatism. *Lithos* **107**, 239–56.

WOODHEAD, J. D. & HERGT, J. M. 2005. A preliminary appraisal of seven natural zircon reference materials for in situ Hf isotope determination. *Geostandards and Geoanalytical Research* **29**, 183–95.

YI, K., CHEONG, C.-S., KIM, J., KIM, N., JEONG, Y.-J. & CHO, M. 2012. Late Paleozoic to Early Mesozoic arc-related magmatism in southeastern Korea: SHRIMP zircon geochronology and geochemistry. *Lithos* **153**, 129–41.